

Magnetic Phase Dependence of the Anomalous Hall Effect in Mn_3Sn Single Crystals

N. H. Sung*, F. Ronning, J. D. Thompson, E. D. Bauer
Los Alamos National Laboratory, Los Alamos, NM 87545, USA

Thermodynamic and transport properties are reported on single crystals of the hexagonal antiferromagnet Mn_3Sn grown by the Sn flux technique. Magnetization measurements reveal two magnetic phase transitions at $T_1 = 275$ K and $T_2 = 200$ K, below the antiferromagnetic phase transition at $T_N \approx 420$ K. The Hall conductivity in zero magnetic field is suppressed dramatically from $4.7 \Omega^{-1}\text{cm}^{-1}$ to near zero below T_1 , coincident with the vanishing of the weak ferromagnetic moment. This illustrates that the large anomalous Hall effect (AHE) arising from the Berry curvature can be switched on and off by a subtle change in the symmetry of the magnetic structure near room temperature.

PACS numbers:

Conducting materials exhibit the Hall effect, a transverse voltage produced by longitudinal current flow in an orthogonally applied external magnetic field. The anomalous Hall effect (AHE), commonly associated with ferromagnets, is governed by extrinsic and intrinsic contributions.¹ The extrinsic contribution depends on details of the impurity scattering, while the intrinsic contribution, first considered by Karplus and Luttinger,² arises from a fictitious magnetic field due to Berry-phase curvature in momentum-space, with a strength determined by the spin-orbit coupling.^{1,3} Experiments show a crossover from a dominant extrinsic effect on the AHE to a dominant intrinsic one with increasing longitudinal resistivity.⁴

Antiferromagnets have recently received attention for potential applications because of their insensitivity to perturbations, no stray fields, and fast spin dynamics that are required for data retention, high-density memory integration, and ultrafast data processing.^{5–7} While an AHE is not realized in collinear antiferromagnets, recent theoretical and experimental investigations of chiral antiferromagnets reveal that a large AHE is possible, even in zero magnetic field, comparable in magnitude to that of ferromagnets.^{8–11} In the hexagonal Mn_3X ($X=\text{Ga}, \text{Ge}, \text{Sn}$) systems (space group $P6_3/mmc$, Fig. 1 (a)), geometrical frustration in the Kagome lattice of Mn atoms within the ab -plane leads to non-collinear antiferromagnetic order with the moments aligned at 120° , forming an inverse triangular spin structure.^{12,13} In the presence of spin orbit coupling, the symmetry of the structure permits an anomalous Hall contribution as well as a finite magnetization, although the relative magnitude of each term can not be determined by symmetry alone. Experimentally, the presence of a weak ferromagnetic moment (WFM)^{13–18} enables the alignment of various domains with a small magnetic field, which otherwise could have opposite AHE contributions. The small coercive field of this weak ferromagnetic state results in large changes to the Hall resistivity ($\approx 10\mu\Omega\text{cm}$) with a small magnetic field ($H_c \approx 500$ Oe) at room temperature.⁹ Large thermal Hall and Nernst signals in Mn_3Sn also arise due to a similar mechanism.^{19,20} These properties may make this material attractive for switches or data storage.

A promising theoretical framework for estimating the

magnitude of the intrinsic AHE based upon details of the band structure shows that the magnitude of the AHE depends sensitively on details of the magnetic and electronic structures.^{5,21–26} Mn_3Sn is well-suited for such an investigation. Neutron diffraction studies on Mn_3Sn revealed the existence of the inverse triangular spin structure below $T_N \approx 420$ K.^{12,13} With this magnetic structure, first principles calculations of the AHE from the Berry curvature are in good agreement with the experimentally determined magnitude of the AHE.^{8,27} It is well known, however, that the magnetic structure of Mn_3Sn depends sensitively on the precise chemical composition and synthesis conditions.^{28,29} A schematic magnetic phase diagram is shown in Fig. 1. Most studies find a transition from the inverse triangular state to an incommensurate magnetic structure below T_1 in which the WFM is also suppressed. T_1 can occur as high as 275 K. A recent magnetic torque study observed two transitions $T_1=275$ K and $T_2=200$ K, which are argued to result from different easy axes in the two spiral magnetic phases.³⁰ At temperatures between 100 and 50 K an increase of the magnetization with decreasing temperature is reported to be due to the onset of spin-glass behavior.^{12,18} The transitions to an incommensurate magnetic structure do not occur in Czochralski grown samples, which are slightly Mn-rich.⁹

Here, we report measurements of the physical properties of Mn_3Sn single crystals, synthesized by the self flux method, to examine the sensitive relation between the AHE and the magnetic structure. In particular, we find a large Hall signal ($\approx -1.5 \sim -3 \mu\Omega\text{cm}$) in the inverse triangular spin state, $T_1 < T < T_N$, which is comparable to that found in other studies.^{9,11} When the magnetic structure becomes an incommensurate spin spiral below $T_1 = 275$ K, the Hall resistivity drops by two orders of magnitude across a first order phase transition. We propose a change in magnetic structure that could account for the sudden vanishing of the AHE. This trait adds to the functionality of large AHE effects in chemically tuned Mn_3Sn .

Mn_3Sn single crystals were grown by the molten-metal flux growth method.³¹ Pieces of Mn (99.98%) and Sn (99.999%) were mixed with an atomic ratio of Mn : Sn = 7 : 3 and placed in an alumina crucible. The crucible

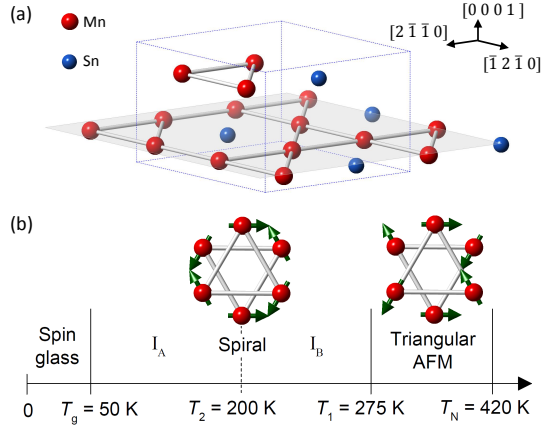


FIG. 1: (a) Crystal structure of Mn_3Sn . Red and blue balls represent Mn and Sn atoms, respectively. Dotted lines indicate the hexagonal unit cell and sticks show the kagome lattice in the $(0\ 0\ 1)$ plane. (b) Schematic magnetic phase diagram and spin structures of Mn_3Sn which indicate the spin glass, spiral, and triangular AFM states as a function of temperature. The $[1\ 1\ \bar{2}\ 0]$ direction and $[0\ 0\ 1]$ direction are easy axes in the spiral spin states, I_A and I_B , respectively.³⁰ Green arrows indicate the suggested in-plane spin structures above and below T_1 . Note the existence of a C_{3z} symmetry below T_1 , which is broken in the inverse spin triangular phase above T_1 . This enables a large AHE above T_1 .

was sealed in a silica tube under vacuum. The tube was heated to 1000 °C at a rate of 100 °C/h, maintained at 1000 °C for 6 hours, and then cooled to 900 °C at a rate of 1.25 °C/h. At 900 °C, the silica tube was centrifuged to separate the crystals from the flux using quartz wool as a filter. Mn_3Sn single crystals were obtained in the form of rods with a hexagonal cross section, with typical dimensions of $\sim 1 \times 1 \times 3\text{ mm}^3$ (Figs. 2 (a) and (b)). The crystals were characterized using Laue and powder x-ray diffractometers, scanning electron microscopy (SEM), and energy-dispersive x-ray spectroscopy (EDX; FEI Quanta 400 FEG-E-SEM) collected at 23 points at various points on the sample surface. DC magnetization measurements of single crystals between 2.5 K and 380 K in magnetic fields up to $H=50\text{ kOe}$ were performed in a Quantum Design Magnetic Property Measurement System (MPMS). Transport measurements were carried out in a Quantum Design Physical Property Measurement System (PPMS) between 1.8 K and 385 K and in magnetic fields up to 90 kOe. 25- μm diameter Pt wires were spot welded to the sample surface to make electrical contacts for electrical resistivity and Hall effect measurements. All Mn_3Sn samples were mechanically polished to remove any remaining flux on the surface before performing the measurements.

The temperature-dependent Hall resistivity (ρ_H) was measured at $H = 10\text{ kOe}$ and $H = 0\text{ Oe}$, and defined as $\rho_H(H=10\text{ kOe}) = [\rho_H(H=10\text{ kOe}) - \rho_H(H=-10\text{ kOe})]/2$ and $\rho_H(H=0\text{ Oe}) = [\rho_H(H \rightarrow +0\text{ Oe}) - \rho_H(H \rightarrow -0\text{ Oe})]/2$,

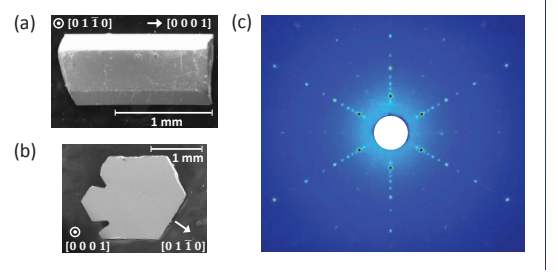


FIG. 2: (Color online) (a) and (b) show SEM images of Mn_3Sn single crystals with indications of crystallographic directions in the samples. (c) Laue pattern of a polished surface showing the $(0\ 0\ 1)$ plane.

respectively. The notation $+0\text{ Oe}$ (-0 Oe) refers to ramping the field to zero from positive (negative) fields ensuring no overshoot. The Hall conductivity in zero field, $\sigma_H(H=0)$ is given by $\sigma_H(H=0) = -\rho_H(H=0)/\rho_{xx}^2(H=0)$ in the limit that the longitudinal electrical resistivity, ρ_{xx} , is much larger than ρ_H . The field dependence of the topological AHE, ρ_H^A , is determined as $\rho_H^A = \rho_H - R_0B - R_s\mu_0M$ where R_0 , R_s and μ_0 are the normal and anomalous Hall coefficients and the permeability, respectively. Here, R_0B and $R_s\mu_0M$ indicate the ordinary Hall effect and the anomalous Hall effect due to magnetism in the compound, while ρ_H^A is the topological Hall effect arising from spin texture due to the Berry phase curvature in momentum space.

Mn_3Sn crystallizes in the hexagonal Ni_3Sn -type structure ($P6_3/mmc$) as shown in Fig. 1 (a). The lattice parameters determined from the powder x-ray diffraction data were $a = 5.6763(4)\text{ \AA}$ and $c = 4.5361(5)\text{ \AA}$ (Fig. S1), comparable to the values found in the previous study.³² The crystallographic directions of the samples are indicated in Figs. 2 (a) and (b), which were determined by Laue diffraction (Fig. 2 (c)). The chemical composition of the samples was determined to be $\text{Mn}_{2.97(1)}\text{Sn}_{1.03(1)}$ based on EDX measurements (Fig. S2), which is close to the ideal chemical composition, and henceforth, we refer to this sample as Mn_3Sn .

The isothermal magnetization, $M(H)$, of a Mn_3Sn single crystal was measured at $T = 5\text{ K}$, 100 K , and 300 K in an applied magnetic field along $H \parallel [0\ 1\ \bar{1}\ 0]$ (Fig. 3 (a)). Weak ferromagnetism with hysteresis was observed at $T = 300\text{ K}$, but the phenomena disappeared at lower temperatures. With an applied magnetic field of $H = 5\text{ kOe}$, the magnetic moment was ~ 11 , 8.5 , and $12\text{ m}\mu_B/\text{f.u.}$ at $T = 5$, 100 , and 300 K , respectively. Therefore, the different magnetic phases were distinguishable from the value of the magnetic moment and the existence of hysteresis in the $M(H)$ curves. Figure 3 (b) shows the temperature dependence of the magnetization divided by field $M(T)/H$, which for simplicity we label as $\chi(T)$, in $H = 1\text{ kOe}$ along the $H \parallel [0\ 1\ \bar{1}\ 0]$ and $H \parallel [0\ 0\ 1]$ directions in a temperature range of $2.5\text{ K} \leq T \leq 380\text{ K}$. Two magnetic phase transitions at $T_1 = 275\text{ K}$ and $T_2 = 200\text{ K}$ were found, which correspond well to previous neutron diffrac-

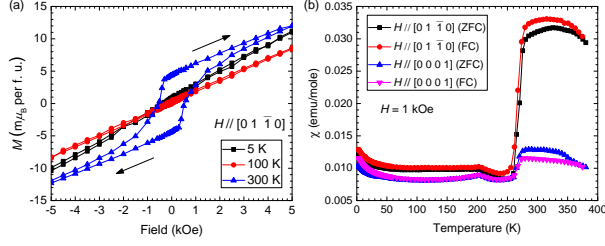


FIG. 3: (Color online) (a) Isothermal magnetization, $M(H)$, of a Mn_3Sn single crystal at $T = 5, 100, 300$ K for $H \parallel [0 1 \bar{1} 0]$. (b) Temperature dependent magnetization divided by field, $M(T)/H$, of a Mn_3Sn single crystal with an applied field of $H = 1$ kOe along $H \parallel [0 1 \bar{1} 0]$ and $H \parallel [0 0 0 1]$ directions, in both ZFC and FC modes.

tion and magnetization measurements results.^{14,33} The change around T_1 is most prominent when the measurements were performed for $H \parallel [0 1 \bar{1} 0]$. The phase transition at T_2 is possibly related to the helical structure reconstruction.³⁰ Below $T_g \approx 50$ K, an upturn in $\chi(T)$ appeared with decreasing temperature and the hysteresis in $\chi(T)$ were observed between zero field cooled (ZFC) and field cooled (FC) temperature sweeps, which indicates a spin-glass state, as previously reported.³⁴ The changes in magnetization at T_1 and T_2 were not observed in $\chi(T)$ measurements of samples that were synthesized using the Bridgman method.^{12,18} Moreover, both transitions were absent in measurements on single crystals synthesized by the Czochralski method using a 10% excess of Mn to account for losses during the growth process; the chemical composition of the Czochralski single crystal was $\text{Mn}_{3.02}\text{Sn}_{0.98}$.⁹ This further confirms that Mn_3Sn samples possess different magnetic structures depending on the chemical composition and/or growth conditions, as previously reported.^{28,29}

The electrical resistivity ρ_{xx} with current I applied along $[0 0 0 1]$ as a function of temperature in zero field exhibits metallic behavior, as shown in Fig. 4 (a), with a residual resistivity ratio ($\rho_{xx}^{385\text{K}}/\rho_{xx}^{2\text{K}}$) of 14. A kink in ρ_{xx} was found at T_1 signaling the transition from the non-collinear AFM to a spiral magnetic state.¹⁷ In the temperature-dependent Hall resistivity (ρ_H) measurement with an applied magnetic field of $H = 1$ T along $H \parallel [0 1 \bar{1} 0]$ and the electrical current along $I \parallel [0 0 0 1]$ (Fig. 4 (b)), an abrupt change was also found at T_1 . A similar, albeit much slower, suppression of the AHE was also observed in ref.¹⁹. The insets of Figs. 4 (a) and (b) show hysteretic behavior of ρ_{xx} and ρ_H vs. T near T_1 upon warming and cooling, which indicates a first-order phase transition at T_1 . A change in sign of ρ_H was observed around T_2 . A slope change in ρ_H around T_g , as shown in Fig. 4 (c), is regarded to be related to the spin-glass state.³⁴ In contrast, Czochralski-grown samples show continuous ρ_{xx} and ρ_H curves without anomalies at the magnetic transitions T_1 and T_2 .⁹ Clearly, the AHE is extremely sensitive to the distinct magnetic structures in Mn_3Sn .

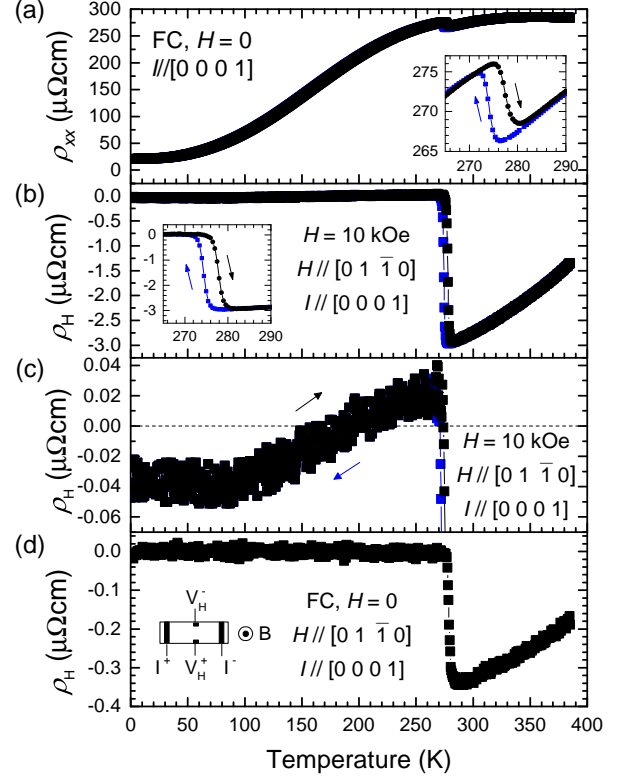


FIG. 4: (Color online) (a) Temperature-dependent zero-field electrical resistivity, $\rho_{xx}(T)$, of Mn_3Sn single crystals with the current along $I \parallel [0 0 0 1]$. (b) Temperature-dependent Hall resistivity, $\rho_H(T)$, of a Mn_3Sn single crystal at $H = 10$ kOe, $H \parallel [0 1 \bar{1} 0]$ and current $I \parallel [0 0 0 1]$; insets: zoom of $\rho_{xx}(T)$ and $\rho_H(T)$ about T_1 . (c) Expanded plot of $\rho_H(T)$. Black circles and blue squares indicate the obtained data as the temperature increases and decreases, respectively. (d) Temperature dependence of the zero-field Hall resistivity obtained after field cooling in a magnetic field of $H = 10$ kOe along $H \parallel [0 1 \bar{1} 0]$ with $I \parallel [0 0 0 1]$ and measuring upon warming. The inset shows the electrical contact configuration for the Hall measurements.

The Hall resistivity, ρ_H , was also measured at zero field ($H=0$) between $2 \text{ K} \leq T \leq 385 \text{ K}$ with increasing temperature and a current along $I \parallel [0 0 0 1]$. The measurements were made after FC in an applied field of $H = 10$ kOe along $H \parallel [0 1 \bar{1} 0]$ direction, then removing the field at the lowest temperature of 2 K (Fig. 4 (d)). In contrast to $\rho_H(10 \text{ kOe})$ shown in Fig. 4 (b), $\rho_H(0 \text{ kOe})$ below T_1 is strictly zero as one would expect for an ordinary metal in zero applied field. Above, T_1 , $\rho_H(0 \text{ kOe})$ has the same functional form as $\rho_H(10 \text{ kOe})$, but with roughly an order of magnitude smaller amplitude than $\rho_H(10 \text{ kOe})$. The origin of this reemergent Hall contribution in zero field requires further investigation. Fig. 5 (a) shows the temperature dependence of the Hall conductivity in zero and 10 kOe fields, $\sigma_H(H=0)$ and

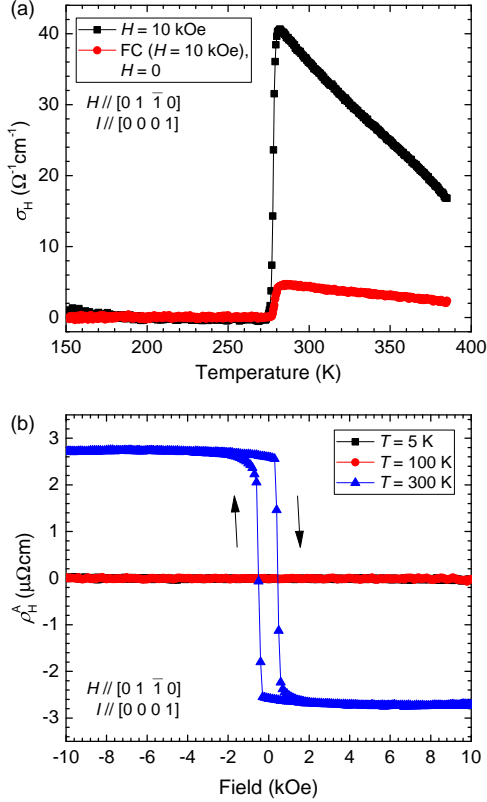


FIG. 5: (Color online) (a) Temperature dependence of the Hall conductivity in zero field, $\sigma_H(H = 0)$, and in a field of 10 kOe, $\sigma_H(H = 10 \text{ kOe})$ obtained from the resistivity data presented in Fig. 4. (b) Magnetic field dependence of AHE, ρ_H^A , at $T = 5, 100, 300$ K. The anomalous Hall contribution is zero below T_1 .

$\sigma_H(H=10 \text{ kOe})$, determined upon warming, where ρ_H was extracted from Figs. 4 (b) and 4 (d), respectively.

In Fig. 5 (b), the field dependence of the intrinsic AHE, ρ_H^A , at $T = 5, 100$, and 300 K is displayed. To obtain ρ_H^A the linear-in-field normal contribution $R_0 B$ was subtracted from the data. From the Hall data in Fig. 4 (b) below T_1 , the absolute value of R_0 is less than $4 \times 10^{-4} \text{ cm}^3/\text{C}$. At 300 K we subtract an extrinsic anomalous contribution with $R_s = -0.6 \text{ cm}^3/\text{C}$ obtained from the linear dependence of ρ_{xy} versus magnetization at 300 K (not shown). These values are comparable in magnitude to those obtained from Czochralski grown crystals,⁹ although the sign of R_s is opposite in the two cases. We note that the values of R_0 and R_s are negligible compared to the intrinsic anomalous Hall contribution above T_1 . The large values of ρ_H^A observed above T_1 are comparable to ferromagnetic Fe or Ni,^{1,4,9} but negligibly small values are found below T_1 . The results for ρ_H^A at room temperature are qualitatively similar although differ slightly in magnitude to previous published results,^{9,11} revealing that details of the electronic structure and/or scattering rate can influence the magnitude of the AHE in the

inverse triangle magnetic state as might be expected.

Though details of the electronic structure determine the magnitude of the intrinsic AHE, the presence or absence of such a term is dictated by symmetry.²⁶ The inverse triangle magnetic state with magnetic ordering wave vector $\mathbf{Q}=0$ at high temperatures in Mn_3Sn breaks the many requisite symmetries to allow an intrinsic AHE contribution. Previous neutron scattering work on Mn_3Sn below T_1 have emphasized the incommensurate magnetic structure, which propagates along the c -axis.^{12,35} Naively, one would expect that an incommensurate magnetic structure would break additional symmetries, and hence it is surprising that the AHE vanishes below T_1 . This suggests that the magnetic structure must fundamentally change to restore a symmetry below T_1 that was absent above T_1 . One such symmetry would be a three-fold rotation about the c -axis (C_{3z}). As shown in Fig. 1, this symmetry is broken above T_1 , but is satisfied in the proposed in-plane magnetic structure below T_1 . The presence of a C_{3z} symmetry forces the Hall conductivity due to the Berry curvature for $H \perp c$ to be identically zero.²⁶ Alternatively, the intrinsic AHE strongly depends sensitively on the orientation of the magnetic structure. Hence, it is conceivable that the incommensurate magnetic structure, could effectively average out the intrinsic AHE to a finite, but small, non-zero value.

Mn_3Sn single crystals synthesized by a simple self-flux method are found to possess a large intrinsic AHE in the so-called inverse triangle magnetic state comparable to that found in crystals grown by other techniques.^{9,11} Importantly, the different synthesis conditions leads to a sharp first order phase transition at 275 K to a new magnetic structure, which causes the intrinsic contribution to the AHE to abruptly vanish. The temperature at which these effects occur are sensitive to growth conditions and/or the Mn:Sn ratio. Consequently, this demonstrates an additional control parameter of the large anomalous Hall effect exhibited by antiferromagnetic Mn_3Sn , which could be exploited for technological applications.

Supplementary Material

See supplementary material for the powder x-ray diffraction and EDX measurements.

Acknowledgments

We thank Priscila Rosa, Hua Chen, Fengcheng Wu, and Ivar Martin for helpful discussions. Work at Los Alamos National Laboratory was supported by the Los Alamos LDRD program. N. H. Sung acknowledges a Director's Postdoctoral Fellowship also through the Los Alamos LDRD program. The EDX measurements were performed at the Center for Integrated Nanotechnologies, an Office of Science User Facility operated for the U.S. Department of Energy (DOE) Office of Science. Los Alamos National Laboratory, an affirmative action

equal opportunity employer, is operated by Los Alamos National Security, LLC, for the National Nuclear Security Administration of the U.S. Department of Energy under contract DE-AC52-06NA25396.

* Corresponding author: nsung@lanl.gov

-
- ¹ Naoto Nagaosa, Jairo Sinova, Shigeki Onoda, A. H. MacDonald, N. P. Ong, *Rev. Mod. Phys.* **82**, 1539 (2010)
 - ² Robert Karplus and J. M. Luttinger, *Physical Review* **95**, 1154 (1954)
 - ³ Di Xiao, Ming-Che Chang, Qian Niu, *Rev. Mod. Phys.* **82**, 1959 (2010)
 - ⁴ T. Miyasato, N. Abe, T. Fujii, A. Asamitsu, S. Onoda, Y. Onose, N. Nagaosa, and Y. Tokura, *Phys. Rev. Lett.* **99**, 086602 (2007)
 - ⁵ Y. Taguchi, Y. Oohara, H. Yoshizawa, N. Nagaosa, Y. Tokura, *Science* **291**, 2573 (2001)
 - ⁶ T. Jungwirth, X. Marti, P. Wadley and J. Wunderlich, *Nature Nanotechnology*, **11**, 231 (2016)
 - ⁷ V. Baltz, A. Manchon, M. Tsoi, T. Moriyama, T. Ono, Y. Tserkovnyak, arXiv:1606.04284
 - ⁸ Yang Zhang, Yan Sun, Hao Yang, Jakub Železný, Stuart P. P. Parkin, Claudia Felser, and Binghai Yan, *Phys. Rev. B* **95**, 075128 (2017)
 - ⁹ Satoru Nakatsuji, Naoki Kiyohara and Tomoya Higo, *Nature* **527**, 212-215 (2015)
 - ¹⁰ Naoki Kiyohara, Takahiro Tomita, and Satoru Nakatsuji, *Phys. Rev. Applied* **5**, 064009 (2016)
 - ¹¹ Ajaya K. Nayak, Julia Erika Fischer, Yan Sun, Binghai Yan, Julie Karel, Alexander C. Komarek, Chandra Shekhar, Nitesh Kumar, Walter Schnelle, Jürgen Kübler, Claudia Felser, Stuart S. P. Parkin, *Sci. Adv.* **2** e1501870 (2016)
 - ¹² P. J. Brown, V. Nunez, F. Tasset, J. B. Forsyth and P. Radhakrishna, *J. Phys.: Condens. Matter* **2**, 9409-9422 (1990)
 - ¹³ Shōichi Tomiyoshi and Yasuo Yamiguchi, *J. Phys. Soc. Jpn.* **51**, 2748-2486 (1982)
 - ¹⁴ Takeo Nagamiya, *J. Phys. Soc. Jpn.* **46**, 787-792 (1979)
 - ¹⁵ T. Nagamiya, S. Tomiyoshi, and Y. Yamaguchi, *Solid State Commun.* **42**, 385-388 (1982)
 - ¹⁶ S. Tomiyoshi, Y. Yamaguchi, Y. Ito, *Physica B: Condensed Matter* **213&214**, 932-934 (1995)
 - ¹⁷ J. W. Cable, N. Wakabayashi, and P. Radhakrishna, *Solid State Commun.* **88**, 161-166 (1993) and J. W. Cable, N. Wakabayashi, and P. Radhakrishna, *Phys. Rev. B* **48** 6159 (1993)
 - ¹⁸ S. Tomiyoshi, S. Abe, Y. Yamaguchi, H. Yamauchi and H. Yamamoto, *J. Magn. Magn. Mater.* **54-57** 1001-1002 (1986)
 - ¹⁹ Xiaokang Li, Liangcai Xu, Linchao Ding, Jinhua Wang, Mingsong Shen, Xiufang Lu, Zengwei Zhu, and Kamran Behnia, *Phys. Rev. Lett.* **119**, 056601 (2017)
 - ²⁰ Muhammad Ikhlas, Takahiro Tomita, Takashi Koretsune, Michi-To Suzuki, Daisuke Nishio-Hamane, Ryotaro Arita, Yoshichika Otani and Satoru Nakatsuji, *Nature Physics*, **13**, 1085 - 1090 (2017)
 - ²¹ Yo Machida, Satoru Nakatsuji, Shigeki Onoda, Takashi Tayama, Toshiro Sakakibara, *Nature* **463** 210 (2010)
 - ²² Hua Chen, Qian Niu, and A. H. MacDonald, *Phys. Rev. Lett.* **112**, 017205 (2014)
 - ²³ Hao Yang, Yan Sun, Yang Zhang, Wu-Jun Shi, Stuart S P Parkin and Binghai Yan, *New J. Phys.* **19** 015008 (2017)
 - ²⁴ Jianpeng Liu and Leon Balents, *Phys. Rev. Lett.* **119**, 087202 (2017)
 - ²⁵ J. Kübler and C. Felser, *EPL*, **108**, 67001 (2014)
 - ²⁶ M. -T. Suzuki, T. Koretsune, M. Ochi, and R. Arita, *Phys. Rev. B* **95** 094406 (2017)
 - ²⁷ Delin Zhang, Binghai Yan, Shu-Chun Wu, Jürgen Kübler, Guido Kreiner, Stuart S P Parkin and Claudia Felser, *J. Phys.: Condens. Matter* **25**, 206006 (2013)
 - ²⁸ G. J. Zimmer and E. Krén, *AIP Conf. Proc.* **5**, 513 (1972)
 - ²⁹ E. Krén, J. Paitz, G. Zimmer, and É. Zsoldos, *Physica B* **80**, 226-230 (1975)
 - ³⁰ T. F. Duan, W. J. Ren, W. L. Liu, S. J. Li, W. Liu, and Z. D. Zhang, *Appl. Phys. Lett.* **107**, 082403 (2015)
 - ³¹ P. C. Canfield and Z. Fisk, *Philos. Mag. B* **65**, 1117-1123 (1992)
 - ³² U. P. Singh, A. K. Pal, L. Chandrasekaran, K. P. Gupta, *Transactions of the Metallurgical Society of Aime* **242**, 1661-1663 (1968)
 - ³³ H. Ohmori, S. Tomiyoshi, H. Yamauchi, H. Yamamoto, *J. Magn. Magn. Mater.* **70**, 249-251 (1987)
 - ³⁴ W. J. Feng, D. Li, W. J. Ren, Y. B. Li, W. F. Li, J. Li, Y. Q. Zhang, and Z. D. Zhang, *Phys. Rev. B* **73** 205105 (2006)
 - ³⁵ J. W. Cable, N. Wakabayashi, and P. Radhakrishna, *J. Appl. Phys.* **75**, 6601 (1994)